

# Investigation of $\text{MAl}_{2-x}\text{Si}_x\text{O}_{4-x}\text{N}_x:\text{Eu}^{2+}$ phosphor for improving luminescence properties of white LEDs

Thanh Binh Ly<sup>1</sup>, Phan Xuan Le<sup>2</sup>

<sup>1</sup>Faculty of Fundamental Science, Industrial University of Ho Chi Minh City, Ho Chi Minh City, Vietnam

<sup>2</sup>Faculty of Mechanical-Electrical and Computer Engineering, School of Engineering and Technology, Van Lang University, Ho Chi Minh City, Vietnam

## Article Info

### Article history:

Received Oct 29, 2021

Revised May 11, 2022

Accepted Jun 19, 2022

### Keywords:

Color homogeneity

Double-layer phosphor

Luminous flux

Monte carlo theory

White light-emitted diodes

## ABSTRACT

We implement a solid-state reaction technique to  $\text{MAl}_{2-x}\text{Si}_x\text{O}_{4-x}\text{N}_x$  ( $M = \text{Ca}, \text{Sr}, \text{Ba}$ ) as well as its variant doped with  $\text{Eu}^{2+}$  at 1300-1400 °C in a nitrogen hydrogen environment. Then, we measure the solubility of  $(\text{SiN})^+$  in  $\text{MAl}_2\text{O}_4$ . By replacing  $(\text{AlO})^+$  with  $(\text{SiN})^+$ , whose solubility is dependent on  $M$  cations, nitrogen may be integrated into  $\text{MAl}_2\text{O}_4$ .  $(\text{SiN})^+$  has poor solubility in  $\text{CaAl}_2\text{O}_4$  ( $x \approx 0.025$ ) and  $\text{SrAl}_2\text{O}_4$  lattices ( $x \approx 0.045$ ) but a considerable integrated quantity of  $(\text{SiN})^+$  against  $\text{BaAl}_2\text{O}_4$  ( $x \approx 0.6$ ). Because of the low solubility of  $(\text{SiN})^+$ , incorporation of  $(\text{SiN})^+$  barely affects the luminescence characteristics of  $\text{MAl}_2\text{O}_4$  when doped with  $\text{Eu}^{2+}$  ( $M = \text{Ca}, \text{Sr}$ ), resulting in discharges in green as well as blue at nearly constant wavelengths measured at 440 as well as 515 nm, respectively. With certain concentrations of  $(\text{SiN})^+$  as well as  $\text{Eu}^{2+}$ ,  $\text{Eu}^{2+}$ -doped  $\text{BaAl}_{2-x}\text{Si}_x\text{O}_{4-x}\text{N}_x$  emits one wide green discharge line under a maximum within the region 500 – 526 nm. Furthermore, once we add nitrogen, both the excitation as well as discharge lines for  $\text{Eu}^{2+}$  exhibit one substantial redshift.  $\text{BaAl}_{2-x}\text{Si}_x\text{O}_{4-x}\text{N}_x:\text{Eu}^{2+}$  is a compelling transmuting phosphor that can be utilized for white light-emitted diodes (WLED) devices because of its efficient stimulation in the range of 390-440 nm radiation.

This is an open access article under the [CC BY-SA](https://creativecommons.org/licenses/by-sa/4.0/) license.



## Corresponding Author:

Phan Xuan Le

Faculty of Mechanical-Electrical and Computer Engineering, School of Engineering and Technology

Van Lang University

Ho Chi Minh City, Vietnam

Email: le.px@vlu.edu.vn

## 1. INTRODUCTION

Because of its significant performance, reliability of chemicals, as well as afterglow properties with substantial duration and brightness,  $\text{Eu}^{2+}$ -doped  $\text{MAl}_2\text{O}_4$  ( $M = \text{Ca}, \text{Sr}, \text{Ba}$ ) would be employed in the form of dependable luminous substances [1]-[3]. The mentioned phosphors were considered suitable in (PDP) plasma display panels and optoelectronics [4], [5]. These phosphors have a bright blue ( $M = \text{Ca}$ ), green ( $M = \text{Sr}$ ), as well as blue-green ( $M = \text{Ba}$ ) fluorescence when exposed to UV and cathode rays. A six-circles form made via corner-sharing  $\text{AlO}_4$  tetrahedra is the foundation to build the three-dimensional formation in  $\text{MAl}_2\text{O}_4$  ( $M = \text{Ca}, \text{Sr}, \text{Ba}$ ). The tetrahedral framework is isostructural, with the tridymite structure in the  $\text{SiO}_2$  polymorph [6]-[8]. The setting as well as the crystallographic locations for cations with two valences inside the channels created via the  $\text{AlO}_4$  rings vary in the different  $\text{MAl}_2\text{O}_4$  structures. In the space group  $P2_1/n$ ,  $\text{CaAl}_2\text{O}_4$  exhibits a monoclinic formation. Three locations of Ca are present in this structure: two of them appear to be sixfold coordinated, while the last one appears to be ninefold coordinated, accompanied by  $\text{O}_2$  particles within one separate channel.  $\text{SrAl}_2\text{O}_4$  and  $\text{BaAl}_2\text{O}_4$  are subject to crystallization within one monoclinic as

well as hexagonal formation with the space groups  $P2_1$  and  $P6_3$ , respectively, for bigger M cations. Both the Sr and Ba ions have ninefold coordination with the oxygen anions and occupy two crystallographic positions in the  $AlO_4$  rings' channels. Although we have substantial research on alkaline-earth aluminates  $MA_2O_4$  treated with  $Eu^{2+}$  (M = Ca, Sr, Ba) [9]-[11] done in the past, still little attention have been paid for improving the performance of these phosphors. Such as replacing Ca with Sr and vice versa [12], [13], by partial substitution of the ion of M as well as Al (e.g, partial substitution of Al with  $B^{12}$ ) or co-dopant trigger ions (e.g,  $Eu^{2+}$  with  $Dy^{3+}$ )<sup>15</sup>. These impacts can improve efficiency, increase the color spectrum of emission, and lengthen the persistence duration. However, we can only customize the excitation as well as absorptivity lines within the ultraviolet limit. Consequently, such materials must undergo stimulation within the UV zone (e.g., less than 350 nm) in order to emit efficiently [14]-[16]. As a result, the excitation bands of  $Eu^{2+}$ -doped  $MA_2O_4$  (M = Ca, Sr, Ba) are inconsistent with the UV blue discharge between 370 and 460 nm created by InGaN-based light-emitted diodes (LED) devices in generating white illumination. For usage in the form of wavelength-transmuting substances to be used in white light-emitted diodes (WLED) devices, significant UV-blue absorptivity (chiefly, 370-460 nm) and extremely high-performamnce transmutation turning blue to green, yellow, as well as red illumination are generally compulsory. As a result, in addition to the aforementioned methods, more innovative ways must be used to produce  $MA_2O_4:Eu^{2+}$  (M = Ca, Sr, Ba) phosphors satisfy such criterias. Alkaline-earth-silicon-nitride as well as oxynitride treated with  $Eu^{2+}$  were recently demonstrated a discharge having a particularly lengthy wavelength as well as excitation inside the observable region of 370-460 nm [17]-[19]. If silicon and nitrogen atoms integrate into  $MA_2O_4$ ,  $MA_{2-x}Si_xO_{4-x}N_x$ :  $Eu^{2+}$  is predicted to expand the lines of excitation towards the observable area as well as discharging under greater wavelengths, especially discharges in yellow as well as green caused by oxide being turned to oxynitride latticework. The integration into  $MA_2O_4$ , for example,  $(AlO)^+$  replacement by  $(SiN)^+$ , would be one reverse procedure responsible for turning nitride to oxynitride, similar to,  $(SiN)^+ \rightarrow (AlO)^+$  replacement in  $Si_3N_4 \rightarrow SiAlON$  and  $Y_2Si_3O_3N_3 \rightarrow Y_2Si_{3-x}Al_xO_{3+x}N_{4-x}$ . The alteration of the framework of  $MA_2O_4:Eu^{2+}$  (M = Ca, Sr, Ba) was proven to be one effective method for improving the luminosity of the material for white-light LED applications [20]-[22].

We studied the existence region of  $MA_{2-x}Si_xO_{4-x}N_x$  substances having packed formation of tridymite and produced undoped and  $Eu^{2+}$ -doped  $MA_{2-x}Si_xO_{4-x}N_x$  ( $0 \leq x < 2$ , M = Ca, Sr, Ba) substances using solid-state process. We use X-ray powder diffraction coupled with Rietveld process to investigate the effect from substituting  $(SiN)^+$  for  $(AlO)^+$  in the case of stage development as well as crystal formation. Finally, we also focus on the luminescence in  $MA_{2-x}Si_xO_{4-x}N_x$  treated with  $Eu^{2+}$  (M = Ca, Sr, Ba) and the relationship between its characteristics and  $Eu^{2+}$  content from  $BaAl_{2-x}Si_xO_{4-x}N_x$  during the study.

## 2. COMPUTATIONAL SIMULATION

To examine the acquired samples, we use X-ray powder diffraction accompanied by Rigaku D/Max- $\gamma$ B diffractometer running under 40 kilovolts, 30 milliamperes having the form of Bragg-Brentano (level graphite monochromator, scintillation counter utilizing) accompanied by Cu  $K\alpha$  radiation. A regular scan at  $2^\circ$  per minute was also employed to confirm phase development. We assessed the parameters of latticework inside the  $2\theta$  limit between  $10^\circ$  and  $90^\circ$  via employing a step-scan mode having step magnitude measured at  $0.01^\circ 2\theta$  along with a counting duration measured at 6 seconds per step, while utilizing silicon powder in the form of an interior standard. We checked the structure of  $BaAl_{2-x}Si_xO_{4-x}N_x$  using the Rietveld technique<sup>23</sup>, utilizing formational characteristics in  $BaAl_2O_4$  as the starting model, assuming both  $Si^{4+}$  and  $N^{3-}$  random distribution across the  $Al^{3+}$  and  $O^{2-}$  sites, respectively, in  $BaAl_2O_4$  to link changes in local structures with luminescence qualities. X-ray diffraction (XRD) data were collected following a step-scan mode having step magnitude measured at  $0.01^\circ 2\theta$  along with a counting duration measured at 15 seconds for each step for the Rietveld refinement. The Rietveld refining functioned with the help of the GSAS program [23]. The proportion, null shift, surroundings, latticework data, apex profile data, fractional coordinates for singular particles, as well as isotropic movement data are among the improved parameters.

We employed a Perkin-Elmer LS-50B luminescence spectrometer accompanied by one Xenon light in the form of excitation source to assess the powder's photoluminescent spectra under room temperature. We employed a red sensitive photomultiplier R928 to observe the radioactivity. The spectra got assessed between 200 and 700 nm under scan rate measured at 100 nm per 60 seconds along with excitation as well as discharge cleavage breadth reaching 2.5 nm. For the excitation spectra, another photomultiplier as well as a ray cleaver managed to rectify them under different light strengths. For rectifying every discharge spectrum, we employed the determined spectra from an adjusted W-light in the form of illumination to investigate the merged influence from the spectrum reaction from the R928 detector as well as monochromator. We utilized white  $BaSO_4$  (~100%) as well as 3% black felt to determine the diffusive reflectance spectra between 230 and 700 nm.

### 3. RESULTS AND DISCUSSION

When creating a white LED, it is imperative to determine the light source's type of your desire. In general, excellent color rendering necessitates emission throughout a substantial portion of the visible spectrum. This feature might be achievable when we put efficiency aside, and vice versa: appropriate (quasi)monochromatic sources can provide extremely high efficiency.

While the purpose of the study is to improve the emission spectrum of LEDs, we should use general illumination applications, both indoors and outdoors. Of course, any visible spectrum, including monochromatic light, might potentially be used for lighting. We, however, focus just on illumination in white, which offers the broadest range of uses. Furthermore, it is an alternative light source for incandescent, quartz-halogen, and compact fluorescent (CFL) bulbs. There are three primary assessment factors to evaluate if the optical spectrum would be acceptable when it comes to universal illumination. Those are the efficiency of the radiation, the illumination's hue output, as well as the lack of dangerous radioactivity. Moreover, when we reconsider the hue output, modern means, including short for color quality score/scale (CQS), appear to replace color rendering index (CRI) [24]. It is significantly more challenging to provide a decent light source for vast lighting. There is no solo relationship between a spectrum and the perceived color since the human eye responds to optical stimuli in such a way. Indeed, two lights that appear to have the same color might have entirely definite emission spectrums. Although the lamps appear to be identical when seen side by side, the devices would still be different, regardless of identical LER values. After having gone over the radiation safety regarding illumination, we will go over the hue output in illumination.

Figure 1 shows the opposite shift in the concentrations of the conversion phosphorus  $\text{MAl}_{2-x}\text{Si}_x\text{O}_{4-x}\text{N}_x: \text{Eu}^{2+}$  ( $M = \text{Ca}, \text{Sr}, \text{Ba}$ ) as well as yellow phosphorus  $\text{YAG:Ce}^{3+}$ . This modification has two meanings: one is to keep average correlation colour temperature (CCT) the same, and second is to keep the influence of the absorptivity as well as dispersion of the WLED device with a pair of phosphor sheets. This adjustment, in turn, impresses the color quality and lumen performance of the said device. The hue quality in the WLED device is thus determined by the  $\text{MAl}_{2-x}\text{Si}_x\text{O}_{4-x}\text{N}_x$  treated with  $\text{Eu}^{2+}$  ( $M = \text{Ca}, \text{Sr}, \text{Ba}$ ) concentration chosen. When the  $\text{MAl}_{2-x}\text{Si}_x\text{O}_{4-x}\text{N}_x: \text{Eu}^{2+}$  ( $M = \text{Ca}, \text{Sr}, \text{Ba}$ ) ratio increased (2%-20% Wt.), the  $\text{YAG:Ce}^{3+}$  content decreased to maintain the median CCTs. Such an effect is also applied on WLED devices under a limit between 5600 K and 8500 K.

Another essential criterion for cutting-edge color conversion phosphors is that the emission spectrum, when combined with the emission of different components (LEDs, other phosphors), results in a true discharge in white yielding a specified hue generation as well as hue temperature. Figure 2 depicts the influence of the phosphor  $\text{MAl}_{2-x}\text{Si}_x\text{O}_{4-x}\text{N}_x: \text{Eu}^{2+}$  ( $M = \text{Ca}, \text{Sr}, \text{Ba}$ ) concentration on the transmitting spectrum in the WLED device. Examining the production criterias will allow us to pick the best option. WLED devices yielding excellent color fidelity lowers luminous flux by a modest amount. As shown in Figure 2, the sum power and the wavelength nearly match throughout the chart. Clearly, the sum power starts to rise in the range among 480-580 nm of this wavelength. After hitting their highest point, both of the indexes decrease continuously and when back to zero at 780 nm. The color consistency in the remote phosphor layout under great temperature can become challenging to regulate.

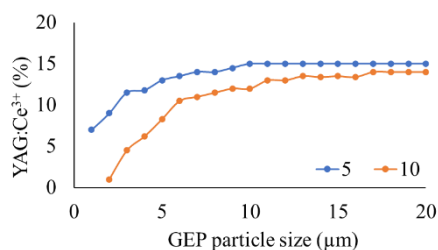


Figure 1. Sustaining median CCT by modifying phosphor content

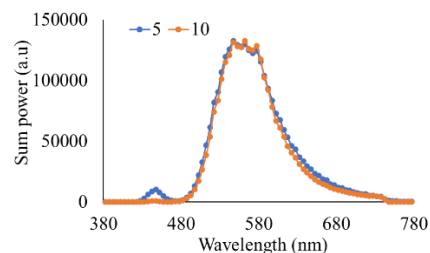


Figure 2. The relation between 4000-K WLED's discharge spectra and  $\text{MAl}_{2-x}\text{Si}_x\text{O}_{4-x}\text{N}_x: \text{Eu}^{2+}$  ( $M = \text{Ca}, \text{Sr}, \text{Ba}$ ) concentration

The efficiency of the emitted light flux of this conversion phosphor layer was further testified to in the article. The results in Figure 3 demonstrate that when the concentration rises, the luminous flux emitted increases considerably. As clearly illustrated from the chart, the climax stays lower than 150 lm, and it remains stable during the process. Due to its excellent characteristics of the discharge reliant on temperature,  $\text{YAG:Ce}^{3+}$  exhibits outstanding reliability of chemical as well as zero degeneration when affected by potent

excitation fluxes confronted in pcLEDs. It is evident from the data in Figure 3 that the broadband emitting rare-earth ions  $\text{Eu}^{2+}$  and  $\text{Ce}^{3+}$  have been extensively researched. Due to their distinct emission characteristics, which include one wide discharge spectrum (responsible for effective hue generation), a modest Stokes shift, and quick decay periods (avoiding saturation). It is possible to achieve high quantum efficiencies and acceptable heat abatement depending on the host material. The discharge spectrum may change from n-UV to deep red depending on the appropriate host chemical.

The color divergence was significantly reduced by the phosphor  $\text{MAI}_{2-x}\text{Si}_x\text{O}_{4-x}\text{N}_x: \text{Eu}^{2+}$  ( $M = \text{Ca}, \text{Sr}, \text{Ba}$ ) concentration in the three average CCTs, as illustrated in Figure 4. The absorptivity in the sheet of red phosphor explains this. The blue illumination from the chip in LED converts into green light when being absorbed by the  $\text{CaAl}_2\text{O}_4:\text{Mn}^{2+}$  phosphor. Beside the blue light, the  $\text{MAI}_{2-x}\text{Si}_x\text{O}_{4-x}\text{N}_x$  treated with  $\text{Eu}^{2+}$  ( $M = \text{Ca}, \text{Sr}, \text{Ba}$ ) particles absorb the yellow light. Due to the material's absorption properties, the chip's blue illumination absorption is more than these two absorbs. The addition of  $\text{MAI}_{2-x}\text{Si}_x\text{O}_{4-x}\text{N}_x: \text{Eu}^{2+}$  ( $M = \text{Ca}, \text{Sr}, \text{Ba}$ ) enhances the green light content in WLEDs, which improves the color uniformity index. Color homogeneity is among the significant characteristics of WLED devices. The more costly the WLED white light, the higher the color homogeneity index. The low cost of  $\text{CaAl}_2\text{O}_4:\text{Mn}^{2+}$ , on the other hand, is a benefit.  $\text{MAI}_{2-x}\text{Si}_x\text{O}_{4-x}\text{N}_x: \text{Eu}^{2+}$  ( $M = \text{Ca}, \text{Sr}, \text{Ba}$ ) may thus be used in a wide range of applications.

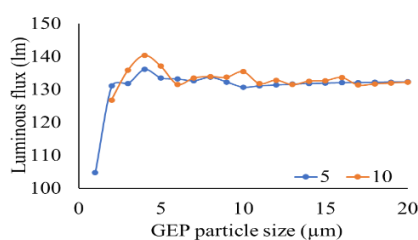


Figure 3. The relation between WLED's lumen and  $\text{MAI}_{2-x}\text{Si}_x\text{O}_{4-x}\text{N}_x: \text{Eu}^{2+}$  ( $M = \text{Ca}, \text{Sr}, \text{Ba}$ ) concentration

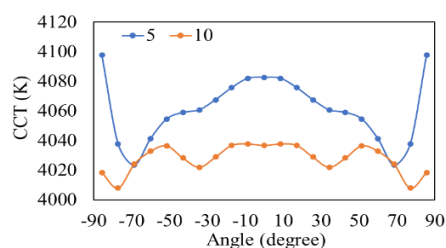


Figure 4. The CCT in WLEDs as a function of  $\text{MAI}_{2-x}\text{Si}_x\text{O}_{4-x}\text{N}_x: \text{Eu}^{2+}$  ( $M = \text{Ca}, \text{Sr}, \text{Ba}$ ) concentration

With CIE proposed during the 90s, using certain main sources for the task of creating certain hues (with hue coordinates designated as  $(x, y)$ ) becomes common, which is the foundation for techniques nowadays, involving merging RGB hues (red, green, along with blue) for the purpose of creating a hue of the triangle, composed using the hue coordinates from RGB. White emission is obtainable if RGB are merged appropriately. RGB and their appropriate hue coordinates will be the sole criteria for the task of creating hue displaying screens. Hence, effective hue generation for discharge would not be challenging to obtain. Greater difficulties are possible if the task is to generate decent illumination. Due to our sight's particular reaction when affected by light, the relation concerning spectrum and detected hue is not simple. A pair of lighting devices may both emit white illumination, while possessing disparate discharge spectrum.

As a result, desirable illumination ought to have a high LER value and excellent hue generation. It is possible to assess LER without ambiguity. On the other hand, the notion of "excellent" hue generation would be still up for discussion. Short for color rendering index (CRI), is the current color rendering standard. It was developed by CIE during 1965 (Ref. 19), revised during 1974 (Ref. 20), then reissued via slight modifications during 1995 (Ref. 21). It would be functional to recap the definition of this CRI for the remainder of the debate. Schanda's excellent work has a detailed discussion of the standard. The hues in items used for testing when lit is compared to the color of test entities when lit via a chosen illumination, which would be obviously critical due to the ability to determine the authentic hues in things. Depending on the test source, an unlimited amount of reference illumination is utilized in the CRI definition: The CCT for the testing illumination is determined by comparing its spectrum to a spectrum in black body radiator, with a temperature (designated as illumination's CCT) highly consistent with the illumination's spectrum. When the CCT for the illumination is less than 5000 K, a radiator with identical CCT plays the role of the reference source for calculating the CRI. Above 5000 K, the CIE (Ref. 23) defines a typical daytime spectrum with identical CCT value obtained via the D65 conventional illuminant. Nonetheless, we found that the CRI definition was no where near being ideal [24]. As such, we suggested various changes, resulting in the development of a different factor during 1996, the universal CRI R96a. On the other hand, said factor is not widely accepted yet. Kumar *et al.* [25] recently presented the most comprehensive set of modifications to the CIE standard, resulting in CQS (short for color quality scale).

Illuminations that are under significant or small CCT value may still provide significant Ra results in the CRI, as long as the reference illumination are under the same CCT. On the other hand, such light sources have a low subjective color rendering ability: they can only reproduce a limited color range, and

colors are seen as artificial. As a result, the CQS assigns these light sources a lower rendering index, generally proportional to the hue scale region with fifteen hue variations. Color uniformity would be only one criterion to consider when assessing WLED color quality. Color quality claimed to be badly affected to color homogeneity index. As a result, recent studies have developed CRI as well as CQS. When light shines upon CRI, it determines the true hue of an object. The unnecessary abundance in green illumination between the principal hues (green, blue, yellow) causes the color imbalance. This has an effect on the color quality of WLEDs, resulting in a decrease in color fidelity. Figure 5 shows that CRI declines in the presence of the remote phosphor  $\text{MAl}_{2-x}\text{Si}_x\text{O}_{4-x}\text{N}_x:\text{Eu}^{2+}$  ( $M = \text{Ca}, \text{Sr}, \text{Ba}$ ) layer. Nonetheless, this outcome is allowed. When comparing CRI with CQS, the CQS is more significant and harder to attain. CQS is an index judged by certain facets, with the first being CRI, the second being the observer's preference, and the third being the color coordinate [25]. With such essential factors, CQS can be seen as a genuine overall assessment for hue output. Figure 6 shows a CQS increase when the  $\text{MAl}_{2-x}\text{Si}_x\text{O}_{4-x}\text{N}_x:\text{Eu}^{2+}$  ( $M = \text{Ca}, \text{Sr}, \text{Ba}$ ) layer is added. When the  $\text{MAl}_{2-x}\text{Si}_x\text{O}_{4-x}\text{N}_x:\text{Eu}^{2+}$  ( $M = \text{Ca}, \text{Sr}, \text{Ba}$ ) concentration rise, CQS does not change considerably when the concentration goes below 10% wt. CRI, along with CQS, diminishes significantly when the concentrations are larger than 10% wt., a result of severe waste of hue if green becomes dominant. Prior to employing  $\text{MAl}_{2-x}\text{Si}_x\text{O}_{4-x}\text{N}_x:\text{Eu}^{2+}$  ( $M = \text{Ca}, \text{Sr}, \text{Ba}$ ), proper concentration selection is critical.

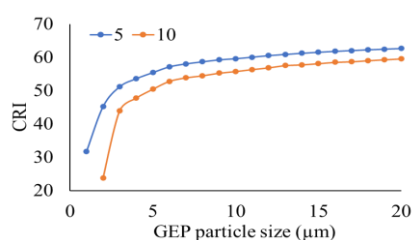


Figure 5. The relation between WLED's CRI and  $\text{MAl}_{2-x}\text{Si}_x\text{O}_{4-x}\text{N}_x:\text{Eu}^{2+}$  ( $M = \text{Ca}, \text{Sr}, \text{Ba}$ ) concentration

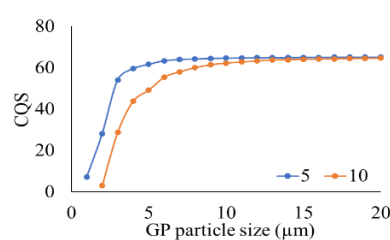


Figure 6. The relation between WLED's CQS and  $\text{MAl}_{2-x}\text{Si}_x\text{O}_{4-x}\text{N}_x:\text{Eu}^{2+}$  ( $M = \text{Ca}, \text{Sr}, \text{Ba}$ ) concentration

#### 4. CONCLUSION

With Ba, Sr as well as Ca mixtures, the maximal solubility for  $(\text{SiN})^+$  in  $\text{MAl}_{2-x}\text{Si}_x\text{O}_{4-x}\text{N}_x$  having the formation of tridymite drops substantially. The solubility for  $(\text{SiN})^+$  within  $\text{CaAl}_2\text{O}_4$  as well as  $\text{SrAl}_2\text{O}_4$  is relatively low [ $x \approx 0.025$  (1.25%) and  $x \approx 0.045$  (2.25%), respectively], but the highest solubility for  $(\text{SiN})^+$  within the  $\text{BaAl}_2\text{O}_4$  latticework would be around  $x \approx 0.6$ , or 30 mol %. As a result, the  $\text{Eu}^{2+}$  emission for Eu-doped  $\text{MAl}_{2-x}\text{Si}_x\text{O}_{4-x}\text{N}_x$  ( $M = \text{Ca}, \text{Sr}$ ) is observed at 440 as well as 515 nm, comparable to the equivalent compounds without nitrogen inclusion. The long-wavelength excitation band of  $\text{BaAl}_{2-x}\text{Si}_x\text{O}_{4-x}\text{N}_x:\text{Eu}^{2+}$  peaks at around 440 nm, leading to a discharge in green under roughly 500 nm to 526 nm while  $x \approx 0.3$ . The redshift owing to nitrogen incorporation can be explained by higher covalency and crystal field splitting when compared to  $\text{BaAl}_2\text{O}_4:\text{Eu}^{2+}$  excitation at approximately 388 nm and emission at about 500 nm. By changing the quantity of  $(\text{SiN})^+$  as well as Eu content, the luminescence characteristics in  $\text{BaAl}_{2-x}\text{Si}_x\text{O}_{4-x}\text{N}_x:\text{Eu}^{2+}$  may be further changed. As a result,  $\text{BaAl}_{2-x}\text{Si}_x\text{O}_{4-x}\text{N}_x:\text{Eu}^{2+}$  has a lot of uses in WLED devices.

#### ACKNOWLEDGEMENTS

This study was financially supported by Van Lang University, Vietnam.




#### REFERENCES

- [1] A. Ferrero, J. L. V. Molinero, A. Pons, and J. Campos, "Index for the evaluation of the general photometric performance of photometers," *Optics Express*, vol. 26, no. 14, pp. 18633-18643, Jul. 2018, doi: 10.1364/OE.26.018633.
- [2] N. Fujimoto, M. Kifune, T. Hara, and N. Akizawa, "The longest transmission experiment of 200 m SI-Plastic optical fibre using a high-luminous Green LED with a new equalizing and carrier sweep out circuit," *OSA Technical Digest*, pp. JTU5A.57, 2018, doi: 10.1364/BGPPM.2018.JTU5A.57.
- [3] W. J. Kim *et al.*, "Improved angular color uniformity and hydrothermal reliability of phosphor-converted white light-emitting diodes by using phosphor sedimentation," *Optics Express*, vol. 26, no. 22, pp. 28634-28640, Oct. 2018, doi: 10.1364/OE.26.028634.
- [4] H. Yang *et al.*, "Giant quantum dots encapsulated inside a freeform lens," *Applied Optics*, vol. 57, no. 35, pp. 10317-10322, Dec. 2018, doi: 10.1364/AO.57.010317.




- [5] X. Li, B. H. Hussain, L. Wang, J. Jiang, and C. P. Yue, "Design of a 2.2-mW 24-Mb/s CMOS VLC receiver SoC with ambient light rejection and post-equalization for Li-Fi applications" *Journal of Lightwave Technology*, vol. 36, no. 12, pp. 2366-2375, Mar. 2018, doi: 10.1109/JLT.2018.2813302.
- [6] X. Ding *et al.*, "Improving the optical performance of multi-chip LEDs by using patterned phosphor configurations," *Optics Express*, vol. 26, no. 6, pp. A283-A292, Mar. 2018, doi: 10.1364/OE.26.00A283.
- [7] E. Robledo *et al.*, "Coregistered and segmented tissue oxygenation maps onto white light images of diabetic foot ulcers," *OSA Technical Digest*, pp. JW3A.44, 2018, doi: 10.1364/TRANSLATIONAL.2018.JW3A.44.
- [8] A. Keller, P. Bialecki, T. J. Wilhelm, and M. Vetter, "Diffuse reflectance spectroscopy of human liver tumor specimens - towards a tissue differentiating optical biopsy needle using light emitting diodes," *Biomedical Optics Express*, vol. 9, no. 3, pp. 1069-1081, Mar. 2018, doi: 10.1364/BOE.9.001069.
- [9] L. Yang, Q. Zhang, F. Li, A. Xie, L. Mao, and J. Ma, "Thermally stable lead-free phosphor in glass enhancement performance of light emitting diodes application," *Appl. Opt.*, vol. 58, no. 15, pp. 4099-4104, May. 2019, doi: 10.1364/AO.58.004099.
- [10] A. M. Nahavandi, M. Safi, P. Ojaghi, and J. Y. Hardeberg, "LED primary selection algorithms for simulation of CIE standard illuminants," *Opt. Express*, vol. 28, no. 23, pp. 34390-34405, Nov. 2020, doi: 10.1364/OE.408754.
- [11] J. H. Kim, B. Y. Kim, and H. Yang, "Synthesis of Mn-doped CuGaS<sub>2</sub> quantum dots and their application as single downconverters for high-color rendering solid-state lighting devices," *Opt. Mater. Express*, vol. 8, no. 2, pp. 221-230, Feb. 2018, doi: 10.1364/OME.8.000221.
- [12] T. P. White, E. Deleporte, and T. C. Sum, "Feature issue introduction: halide perovskites for optoelectronics," *Opt. Express*, vol. 26, no. 2, pp. A153-A156, Jan 2018, doi: 10.1364/OE.26.00A153.
- [13] Z. Zhao, H. Zhang, S. Liu, and X. Wang, "Effective freeform TIR lens designed for LEDs with high angular color uniformity," *Applied Optics*, vol. 57, no. 15, pp. 4216-4221, May. 2018, doi: 10.1364/AO.57.004216.
- [14] H. Yu *et al.*, "Solar spectrum matching with white OLED and monochromatic LEDs," *Applied Optics*, vol. 57, no. 10, pp. 2659-2666, Apr. 2018, doi: 10.1364/AO.57.002659.
- [15] N. Anous, T. Ramadan, M. M. Abdallah, K. A. Qaraq, and D. Khalil, "Impact of blue filtering on effective modulation bandwidth and wide-angle operation in white LED-based VLC systems," *OSA Continuum*, vol. 1, no. 3, pp. 910-929, Nov. 2018, doi: 10.1364/OSAC.1.000910.
- [16] H. Ke *et al.*, "Lumen degradation analysis of LED lamps based on the subsystem isolation method," *Applied Optics*, vol. 57, no. 4, pp. 849-854, Feb. 2018, doi: 10.1364/AO.57.000849.
- [17] Z. Huang *et al.*, "Towards an optimum colour preference metric for white light sources: a comprehensive investigation based on empirical data," *Opt. Express*, vol. 29, no. 5, pp. 6302-6319, Mar. 2021, doi: 10.1364/OE.413389.
- [18] R. Fan, S. Fang, C. Liang, Z. Liang, and H. Zhong, "Controllable one-step doping synthesis for the white-light emission of cesium copper iodide perovskites," *Photon. Res.*, vol. 9, no. 5, pp. 694-700, Apr. 2021, doi: 10.1364/prj.415015.
- [19] X. Xi *et al.*, "Chip-level Ce:GdYAG ceramic phosphors with excellent chromaticity parameters for high-brightness white LED device," *Opt. Express*, vol. 29, no. 8, pp. 11938-11946, Apr. 2021, doi: 10.1364/OE.416486.
- [20] J. R. Beattie, and F. W. L. E. White, "Exploration of principal component analysis: deriving principal component analysis visually using spectra," *Appl. Spectrosc.*, vol. 75, no. 6, pp. 361-375, Jan. 2021, doi: 10.1177/0003702820987847.
- [21] Y. Wang *et al.*, "Tunable white light emission of an anti-ultraviolet rare-earth polysiloxane phosphors based on near UV chips," *Opt. Express*, vol. 29, no. 6, pp. 8997-9011, Mar. 2021, doi: 10.1364/OE.410154.
- [22] A. Udupa, X. Yu, L. Edwards, and L. L. Goddard, "Selective area formation of arsenic oxide-rich octahedral microcrystals during photochemical etching of n-type GaAs," *Opt. Mater. Express*, vol. 8, no. 2, pp. 289-294, Feb. 2018, doi: 10.1364/OME.8.000289.
- [23] X. Li *et al.*, "Highly stable and tunable white luminescence from Ag-Eu<sup>3+</sup> co-doped fluoroborate glass phosphors combined with violet LED," *Opt. Express*, vol. 26, no. 2, pp. 1870-1881, Jan. 2018, doi: 10.1364/OE.26.001870.
- [24] K. Werfli *et al.*, "Experimental demonstration of high-speed 4 × 4 imaging multi-CAP MIMO visible light communications," *J. Lightwave Technol.*, vol. 36, no. 10, pp. 1944-1951, Jan. 2018, doi: 10.1109/JLT.2018.2796503.
- [25] S. Kumar, M. Mahadevappa, and P. K. Dutta, "Extended light-source-based lensless microscopy using constrained and regularized reconstruction," *Appl. Opt.*, vol. 58, no. 3, pp. 509-516, Jan. 2019, doi: 10.1364/AO.58.000509.

## BIOGRAPHIES OF AUTHORS



**Thanh Binh Ly**    received a Environmental Engineering Technology Master degree from the Industrial University of Ho Chi Minh City, in 2020. Currently, He is research Industrial University of Ho Chi Minh City, Vietnam. Her research interests include simulation LEDs material, renewable energy. She can be contacted at email: lythanhbinh@iuh.edu.vn.



**Phan Xuan Le**    received a Ph.D. in Mechanical and Electrical Engineering from Kunming University of Science and Technology, Kunming city, Yunnan province, China. Currently, He is a lecturer at the Faculty of Engineering, Van Lang University, Ho Chi Minh City, Vietnam. His research interests are Optoelectronics (LED), power transmission and automation equipment. He can be contacted at email: le.px@vlu.edu.vn.